Computation of ocean-like surface thermal emission and bistatic scattering with the reduced local curvature approximation

Joel T. Johnson, *Senior Member, IEEE,* and Tanos M. Elfouhaily

***Abstract*— The reduced local curvature approximation of third order (RLCA3) is a recently proposed model for rough surface scattering that matches the Kirchhoff Approximation as well as the first and second order small perturbation method (SPM) in appropriate limits. Predictions of bistatic scattering, thermal emission, and reflected atmospheric brightnesses from the RLCA3 model are presented in this paper through a Monte Carlo simulation process. The surfaces considered are realizations of an ocean-like spectrum, and contain features ranging from 64 to 0.5 electromagnetic wavelengths. Results are compared with predictions from the commonly applied "two-scale" theory of sea emission, as well as results from a previous similar study using the small slope approximation (SSA) of Voronovich. Results show a high level of agreement between RLCA3 and SSA predicted bistatic scattering patterns, but appreciable differences in predicted surface brightnesses, particularly in the third Stokes parameter.**

I. Introduction

Interest in the computation of microwave polarimetric thermal emission from the sea surface has recently increased due to the availability of satellite data from the WindSAT mission [1]. A theory of sea emission can be developed based on existing theories of scattering from the sea surface in combination with Kirchhoff's law of thermal emission. The "two-scale" theory of scattering from the sea surface extended in [2] to compute polarimetric sea brightnesses has become the most commonly applied method. A recent study [3] examined emission predictions of the small-slope approximation (SSA) method of Voronovich [4]-[5] through a Monte Carlo computational process using ocean-like surfaces. Results of the study showed reasonable agreement between SSA and "two-scale" model predictions, although measurable differences between the two models were observed, particularly in the third Stokes parameter brightness, which had a significantly reduced amplitude in the SSA compared to two-scale predictions. A complete validation of either model's predictions awaits the development of numerical methods that are accurate and efficient enough to perform the required large-scale computations.

Recently, a new model of rough surface scattering called the "reduced local curvature approximation of third order" (RLCA3) has been developed [6]. The model has a functional form identical to the SSA, but with modified kernel functions, and expresses surface scattered fields in terms of a series of terms in "curvature order" of the surface. The first series term is equal to the Kirchhoff Approximation (KA) for scattered fields, while the second field series term corrects the first term to allow agreement with the small perturbation method (SPM) when appropriate. When two field series terms are included, the model matches the Kirchhoff approximation (KA) in the high frequency limit as well as the SPM up to second order in the low frequency limit. The model also captures a first order in slope tilt invariance of the first order SPM. These properties are similar to the SSA, but recent works have shown that the SSA in fact fails to achieve agreement with KA in the high frequency limit for penetrable surface boundary conditions [7]-[8].

The RLCA3 model was derived from an initial formulation of the "local curvature approximation" (LCA) in [9] and an extension of the LCA to improve its tilt invariance properties [10]. Reference [9] also presents another model called the "weighted curvature approximation" (WCA); the WCA matches the SPM to first order only as well as the KA while requiring only a single field series term. While predictions of in-plane bistatic scattering have been explored using the LCA/WCA models [9]-[11], no references have reported computations of out-of-plane bistatic scattering or thermal emission using these models. Because it is well known that inclusion of second order SPM contributions is required to ensure power conservation for small height surfaces, and because power conservation is critical in producing accurate brightness temperature predictions, only models that include the second order SPM limit when appropriate are recommended for studies of ocean-like surface emission.

In this paper, the RLCA3 model is applied to compute complete rough surface bistatic scattering patterns as well as direct surface thermal emission and reflected atmospheric emission. Results are compared primarily with the SSA, as the distinction between the RLCA3 and SSA theories is of interest, but thermal emission results are also compared with two-scale model predictions. Due to the similarity of the RLCA3 and SSA models, the process used to compute brightnesses is essentially identical to that described in [3]: a Monte Carlo simulation involving a deterministic surface RLCA3 formulation. This approach is more computationally efficient than use of analytically averaged cross section expressions for the cases of interest.

The next section provides a brief review of the formulation and computational process, while Section III presents com-

Manuscript received Month dd, yyyy; revised Month dd, yyyy. T. M. Elfouhaily is with the Rosenstiel School of Marine and Atmospheric Science, University of Miami. J. T. Johnson is with The Ohio State University, Dept. of Electrical and Computer Engineering and ElectroScience Laboratory.

parisons of RLCA3 and SSA predicted bistatic scattering patterns. Section IV then compares predicted surface brightness temperatures and reflected atmospheric brightnesses from the RLCA3, SSA, and two-scale theories.

II. Formulation and computations

The computation of surface brightness temperatures through Kirchhoff's Law requires an integration over surface bistatic scattering cross sections. Determination of average surface brightness temperatures in the RLCA3 model therefore requires computation of the average value of the complete bistatic scattering pattern. The approach developed in [3] for performing these computations involves a Monte Carlo simulation of the RLCA3 using periodic surfaces. Through the algorithm described in [3], RLCA3 scattered fields at a single bistatic scattering angle for a specific surface can be obtained in the order of N operations, where N is the number of points contained in the discretized surface profile. The required discretization of the surface profile limits the range of surface scales that are considered. Because resolution of the "Bragg" portion of the sea spectrum is important for brightness computations, the surface must be sampled on a sub-wavelength scale, and the range of "large-scale" surface features that can be resolved becomes limited by computational requirements.

The use of periodic surfaces also results in a discretized scattered field (i.e. the "Floquet modes"), so that the Kirchhoff's Law integration over scattered angles becomes discretized. When surface periods large compared to the electromagnetic wavelength are used, this discretization becomes sufficiently fine to approximate scattering from a continuous surface.

A. Bistatic scattering patterns

Because the RLCA3 computation includes two field series, three contributions to scattered powers result (the power in each field series term, and the correlation between the two.) The contribution of the first term will be labeled as "KA" in what follows (since the first field series term is the Kirchhoff approximation), while the sum of the first and second terms will be labeled "LCA3" (similar to the "SSA3" description used in [3]), and the sum of all three terms "LCA4". Note that the final term properly includes contributions from both the second and third RLCA3 field series terms; however the third RLCA3 field series term is not known at present for penetrable surfaces, and is therefore not considered in this study. Due to this limitation, comparisons of "LCA3" and "LCA4" power results can provide only incomplete information on convergence. Bistatic scattering patterns will be shown in terms of normalized radar cross section (NRCS) values in decibels, and will include the contributions of all three cross section terms. Polarization dependencies of the NRCS are specified through an $\alpha\beta$ notation, with α and β chosen from H or V for horizontal or vertical polarizations, respectively, and with α and β representing the scattered and incident polarizations, respectively.

B. Brightnesses

Surface brightness temperatures can be determined from the bistatic scattering pattern through Kirchhoff's law of thermal emission; see [3] for a detailed formulation. Polarimetric brightnesses are labeled as T_h, T_v, U, and V, where T_h and T_v refer to brightness temperatures in the horizontally and vertically polarized channels, respectively, while U and V refer to the real and imaginary parts of the correlations between horizontal and vertical received fields, respectively. The U and V brightnesses are also referred to as the third and fourth Stokes brightnesses in what follows. The physical temperature of the sea surface is assumed to be 285 K. The terms "KA", "LCA3", and "LCA4" again will be used to refer to partial sums of the three brightness terms.

Typical models of the sea surface spectrum include only constant and second azimuthal harmonic variations in azimuth. It has been shown [12] that the resulting brightness temperatures are of the form

$$\begin{bmatrix} T_h \\ T_v \\ U \\ V \end{bmatrix} \approx \begin{bmatrix} T_{h0} + T_{h2}\cos 2\phi_i \\ T_{v0} + T_{v2}\cos 2\phi_i \\ U_2 \sin 2\phi_i \\ V_2 \sin 2\phi_i \end{bmatrix} \tag{1}$$

where ϕ_i denotes the azimuth angle between the radiometer look direction and the wind direction. Although a first azimuthal harmonic variation is also observed in experimental data, simple Gaussian random process models of the sea surface cannot capture the associated up/down wind asymmetries of the surface [13]. Because a Gaussian random process model of the sea surface is used in this study, only the zeroth (i.e. T_{h0} and T_{v0}) and second (i.e. T_{h2}, T_{v2}, U_2, and V_2) azimuthal harmonics are of interest. The second azimuthal harmonics typically capture brightness variations due to any up/cross wind asymmetries of the surface.

C. Reflected atmospheric power

Reflections of downwelling atmospheric brightness into the radiometer observation direction represent a significant contribution to total observed brightnesses. Given the bistatic scattering pattern of a surface, it is straight forward to perform an integration over the bistatic scattering pattern weighted by the atmospheric downwelling brightness at a specific angle; for details refer to [3]. In the results to be shown, a simple one-layer model of downwelling atmospheric brightness is used:

$$T_{atm}(\theta) = T_A\left(1 - \exp\left[-\tau \sec\theta\right]\right) \tag{2}$$

Here T_A is set to 285 K, and τ represents the zenith opacity of the atmosphere in Nepers. Results will be shown for τ values ranging from 0.01 to 0.5; specular atmospheric brightnesses (i.e. $T_{atm}(\theta_i)$) then range from 4.9 to 165.8 K with $\theta_i = 55^\circ$.

D. Computational issues

The parallel computing approach described in [3] is applied to allow computations to be performed for the large number of fields (approximately 12800 scattering angles) in the bistatic scattering pattern. In this algorithm, the set of scattered fields for a given surface realization is divided among

16 processors. To capture brightness variations with azimuthal angle, computations were performed for azimuth observation angles of 0, 30, 60, and 90 degrees; the results were then used to extract the zeroth and second azimuthal harmonic terms when necessary. The final parallel simulation used 64 processors, composed of groups of 16 processors used for each of the four azimuthal angles considered. Results were obtained using supercomputing resources at the Maui High Performance Computing Center (MHPCC) [14]. A typical 64 processor run utilized 10 surface realizations; the computing time required was on the order of 2 CPU hours for each node. A total of 50 realizations were included in computing the final averages shown, with brightness results showing standard deviations typically less than 0.2 K.

E. Specific cases considered

The results considered here used surfaces of 64λ by 64λ, where λ is the electromagnetic wavelength, sampled into 256 by 256 points. This surface size was selected as a compromise between the computational resources available and the desire to simulate as large an ocean-like surface as possible. Surface length scales shorter than $\lambda/2$ were also removed in the simulation, in order to avoid aliasing issues in the RLCA3 computation. When considering true sea surfaces, 64λ at microwave frequencies captures only a small portion of the "long-wave" region; however this portion should be sufficient to produce some of the long-wave "tilting" effects predicted by the two-scale model, so that the basis of this two-scale approximation can be investigated. Simulations were also performed for a second set of 64λ by 64λ surfaces, in which surface length scales larger than 4λ were additionally removed. In this case, large scale "tilting" effects should be minimized, and total surface height will be small compared to the wavelength. This set of surfaces will be termed the "small height" case, while the former set will be termed the "large height" case in what follows.

The surfaces used were Gaussian random processes generated using the "Durden-Vesecky" spectrum described in [2], [3], and [15]. This spectrum was selected because it has been applied in numerous studies of ocean-like surface thermal emission, although of course there are numerous sea spectral models that could be considered, none of which has been validated as a complete description of true sea surfaces. The spectrum parameters $a_0 = 0.008$, $d = 0.4789$, and $b_0 = a_0$ [2] were used. A fixed wind speed of $U_{19.5} = 10$ m/sec is considered in the results of Sections III-IV; note the limitation of surface length to 64λ results in a much smaller surface rms height than a true sea surface at 10 m/sec windspeed. For this reason, investigating variations with wind speed in this simulation is not realistic. A fixed observation angle of 55 degrees (similar to many satellite radiometers) is used, along with a frequency of 19.35 GHz and a sea water relative permittivity of $29.41 + i35.98$.

III. Bistatic scattering patterns

Figures 1-4 illustrate comparisons of RLCA3 and SSA (both including all three power contributions) NRCS predictions for both small (plots (a)-(c) in each figure) and large (plots (d)-(f)) surface height cases. NRCS values in decibels are shown as a gray-scale image over the upper scattered hemisphere and for $\phi_i = 0$ degrees. In these figures, the incident field approaches from the left at 55 degrees polar incidence angle; the largest NRCS values are observed in the specular region for the large height case, as should be expected. Plots (c) and (f) are gray-scale images of the difference between the RLCA3 NRCS in decibels and the SSA NRCS in decibels.

Plots (a)-(c) of Figures 1-4 show scattering behaviors typical for ocean-like surfaces truncated to include only the "short wave" portion of the sea spectrum. Under the first-order SPM (which should be very accurate for these small height surfaces), near specular scattering is directly proportional to the surface spectrum evaluated at small values of the wavenumber. Since the spectrum is zero for these length scales, an "excluded" region surrounding the specular direction results in these plots; similar scattering effects with truncated surfaces were observed using a numerical model in [16]. The coherent reflected wave is observed as the small bright point within this excluded region. Typical behaviors associated with bistatic Bragg scattering are observed, including small values of HH cross sections for scattering into directions rotated 90 degrees in azimuth from the plane of incidence, small values of cross polarized cross sections in the plane of incidence, and an interesting minimum in VV bistatic scattering over a near circular region. The last phenomenon has not had extensive discussion in the literature, but could have importance in some sea scattering applications. Differences between SSA and RLCA3 predictions are generally small (well within the 2 dB colorscale), with the exception of HH cross sections at backward polar scattering angles close to 90 degrees. Here RLCA3 predictions exceed those of the SSA by up to 10 dB in some cases. A comparison of these predictions with those from an SPM computation up to 4th order shows the RLCA3 results to be in error in this region. These errors are caused by a "shadowing" effect in the RLCA3 kernel function that occurs for large incidence or scattering angles [10]. While the RLCA3 meets the SPM limit analytically, the surface heights required to produce this agreement grow smaller as either grazing incidence or scattering is approached. However the effect of these differences on brightnesses will be found to be minimal in Section IV.

Results for the large surface height case in plots (d)-(f) show similar behaviors, except that the near specular excluded region is no longer present due to the inclusion of large surface scale features. A broad specular scattering pattern results instead in both co-polarized cases, combined with lower scattering levels in the cross-polarized results. Other features of the plots remain similar, including the large differences between RLCA3 and SSA predictions for HH backward traveling cross sections at large polar scattering angles. A validation of either model's predictions in the latter case await numerical computations for the large height surface parameters, but again, it will be shown in Section IV that the two theories at least produce similar horizontally polarized brightnesses. Other differences between the models are generally increased, up to around 5 dB maximum values in VV,

HV, and VH polarizations, but the difference plot shows no consistent trend of these differences versus scattering angle, so that the increased randomness of the large height case is the source of these larger differences.

Overall these comparisons confirm that the SSA and RLCA3 models yield similar predictions of bistatic scattering patterns for the surfaces considered, with the exception of the HH differences described above.

IV. Surface and reflected atmospheric brightnesses

Figure 5 examines direct surface emission predictions in the "large height" surface case from the RLCA3 theory as the KA, LCA3, and LCA4 power terms are included. Variations with azimuthal angle in the four polarimetric quantities are illustrated in the four sub-plots. Results show a significant change between KA, LCA3, and LCA4 predictions. In particular, the KA theory under predicts linearly polarized brightnesses, and obtains an incorrect sign for the U brightness. Average values of the linear brightnesses also change significantly from LCA3 to LCA4. Similar trends with smaller but still non-negligible changes (not shown) are observed for the small height case. Note KA brightnesses at 30 and 60 degrees azimuth angle in Figure 5 are not precisely equal in the polarimetric channels; the small differences observed are due to the finite number of realizations included in the Monte Carlo simulation, and the small polarimetric brightnesses predicted. Overall, these results demonstrate that use of both RLCA3 field series terms is critical for predicting surface polarimetric brightnesses; this might be expected given the fact that the second order SPM kernel must be included in computing rough surface brightnesses in the SPM theory in order to obtain a realistic prediction. Note the relatively large azimuthal harmonic variations produced by short scale sea waves only, due to the strong azimuthal asymmetry of short waves in the Durden-Vesecky spectrum.

Brightness predictions of the RLCA3 theory (including all three power contributions) were compared with the SPM for the small height surface case. Results (not plotted) showed RLCA3 and SPM computations to match to within 0.2 K. This agreement validates the reduction of the RLCA3 theory to the second order SPM limit for small height surfaces, even given the differences in HH bistatic cross sections discussed in Section III.

Figure 6 compares direct surface emitted RLCA3 brightnesses with predictions of the two-scale theory of [2], the SPM, and the SSA for the large height case. Both RLCA3 and SSA brightnesses in the Figure include all three power term contributions. Two-scale model predictions (analytically averaged) were computed for continuous surfaces, but using identical parameters to the RLCA3 simulation, including truncation of surface length scales to a maximum of 64λ. The two-scale "cutoff wavenumber" was chosen as the electromagnetic wavelength divided by 5, i.e. sea surface waves longer than 5 electromagnetic wavelengths were classified as "large scale" features.

Results show RLCA3 and SSA predictions to be very similar in horizontal and fourth Stokes' parameter channels, with both predicting larger horizontal brightnesses than either the SPM or two-scale theories. RLCA3 predictions of the vertical brightness are appreciably larger (around 1.5 K) than those of the SSA, with two-scale model predictions falling in between the two and the SPM obtaining the largest vertically polarized brightnesses. The SSA also predicts a significantly larger vertically polarized azimuthal variation than the other theories. For the third Stokes' parameter, the SSA model yields values significantly smaller than all other theories, as discussed in [3]. RLCA3 predictions however are closer to those of the two-scale and SPM. In order to examine the difference between maximum U brightness predictions, RLCA3 and SSA results at 45 degrees azimuthal angle were also computed, and are included in the plots.

While these results do not conclusively establish a superior theory of sea brightnesses, overall the comparisons suggest that the RLCA3 method yields a reasonable prediction of sea surface brightnesses. The theories considered all yield slight brightness differences that are a function of the polarization considered. The larger amplitudes of third Stokes' parameter brightnesses obtained from the RLCA3 model yields further credence to the belief that the SSA theory may have reduced accuracy for this channel.

A. Reflected atmospheric brightness

Because reflected atmospheric brightnesses were computed as both a function of azimuth angle and the zenith attenuation τ, it is most convenient to plot reflected brightness zeroth and second azimuthal harmonics versus τ. Due to the large change in reflected atmospheric brightnesses with the zenith attenuation τ, it is most convenient to plot results for the zeroth azimuthal harmonics in terms of differences between models, rather than the predicted values of individual models. Accordingly, zeroth harmonic plots will be illustrated as RLCA3 and SSA predictions minus predictions of the two-scale theory. Zeroth azimuthal harmonic predictions of the two-scale theory for the small and large height cases are not shown here, but are available in [3].

For the small surface height case, the RLCA3 showed excellent agreement with the SPM (zeroth harmonics within 0.2 K over a wide range of atmospheric conditions), again verifying the reduction of the RLCA3 theory to the SPM limit (results not shown). Figure 7 illustrates RLCA3 reflected atmospheric zeroth harmonics minus predictions of the two-scale model for the large height cases. Larger differences with two-scale model predictions up to 1.2 K are observed. Differences are larger in horizontal polarization, and the two-scale theory obtains larger values than the RLCA3 in both polarizations. As with surface brightnesses, RLCA3 predictions are close to SSA predictions for horizontal polarization, but closer to the SPM for vertical polarization. While the differences observed are non-negligible, a disagreement of only ≈ 1.2 K out of atmospheric reflected brightnesses ranging up to 165K can be considered very good agreement between these theories. The SPM reflected brightnesses shown were computed using power equations similar to those of the RLCA3, but based on the first order SPM solution for non-specular bistatic scattering

cross sections and the second order SPM solution for specular reflection. The degree of agreement between the RLCA3 and SPM results is remarkable in the large surface height case, because, unlike the case of direct surface emission, there is no guarantee of a "small slope" behavior for reflected atmosphere computations from the SPM.

Second azimuthal harmonic variations of reflected brightnesses were also compared between the RLCA3 and SPM theories in the small height surface case. Again the two theories showed excellent agreement (values within 0.2 K). Figure 8 plots second azimuthal harmonics of the reflected brightness for the large height case. Results from a simple approximate method for reflected brightnesses (labeled "approx" in the Figure) that assumes a uniform atmospheric brightness (see [3]) are also included based on two-scale model predictions. Results show RLCA3, SSA, two-scale, and SPM predictions to be similar in most respects, although the SSA continues to obtain smaller predictions of the third Stokes' parameter than the other models. The simple approximation provides reasonable predictions of U and V brightnesses, but has large errors in the linear brightness channels. In particular, the sign of linear channel second azimuthal harmonics is incorrectly predicted by this approximation, showing that atmospheric contributions increase, rather than decrease, total brightness azimuthal variations for these channels.

V. Conclusions

As in [3], the results of this study show that the RLCA3 model yields predictions similar to those of the "active" SSA, two-scale, and "passive" SSA (i.e. SPM) models. The high level of agreement obtained with SPM in the small height case validates the reduction of RLCA3 to the second order SPM limit. The level of error observed among theories in the larger height case is significant, so that questions remain regarding the absolute accuracy of all the theories considered. RLCA3 predictions of third Stokes' parameter brightnesses however did not show the unusually small values obtained from the active SSA, suggesting that the active SSA theory may have less accuracy in this case. Of course, these conclusions likely depend on the particular sea surfaces simulated, as well as the particular observation angle (55°) used.

Although neither the RLCA3 nor the active SSA theories require use of a cutoff wavenumber, the overall accuracy of these theories for scattering cross sections is not established, particularly as grazing scattering angles are approached. Further studies will be required to address absolute accuracy issues, and as numerically exact predictions become more available progress should be possible. It should be noted that uncertainties in the sea surface spectrum, sea water permittivity, and other geophysical parameters may result in errors that dominate those from the electromagnetic model when applied to satellite data; model "tuning" based on matching satellite data will be required to develop effective spectrum and permittivity models. The basic qualitative agreement between the electromagnetic methods considered indicates that such tuning based on any of the these methods should produce at least a reasonably accurate physically based forward model.

VI. Acknowledgments

This work was performed under the support of the Naval Research Laboratory and the National Polar-Orbiting Operational Environmental Satellite System (NPOESS) Integrated Program Office. Use of IBM SP supercomputing resources at the Maui High Performance Computing Center is also acknowledged.

References

[1] Gaiser, P. W. et al, "The WindSAT spaceborne polarimetric microwave radiometer: sensor description and early orbit performance," *IEEE Trans. Geosc. Remote Sens.*, vol. 42, pp. 2347-2361, 2004.

[2] Yueh, S. H., "Modeling of wind direction signals in polarimetric sea surface brightness temperatures," *IEEE Trans. Geosc. Remote Sens.*, vol. 35, pp. 1400-1418, 1997.

[3] Johnson, J. T., "A study of ocean-like surface thermal emission and reflection using Voronovich's small slope approximation," *IEEE Trans. Geosc. Rem. Sens.*, vol. 43, pp. 306–314, 2005.

[4] Voronovich, A. G., *Wave Scattering from Rough Surfaces*, Berlin: Springer-Verlag, 1994.

[5] Voronovich, A. G., "The effect of the modulation of Bragg scattering in small-slope approximation," *Wave Random Media*, vol. 12, pp. 341–349, 2002.

[6] T. M. Elfouhaily and J. T. Johnson, "A new model for rough surface scattering," submitted to *IEEE Trans. Geosc. Rem. Sens.*, 2006.

[7] M. S. Gilbert and J. T. Johnson, "A study of the higher-order small slope approximation for 3-D scattering from a dielectric Gaussian rough surface," *Waves Random Media*, vol. 13, pp. 137–149, 2003.

[8] C.-A. Guérin and M. Saillard, "On the high-frequency limit of the second-order small-slope approximation," *Waves in Random Media*, vol. 13, pp. 75–88, 2003.

[9] T. Elfouhaily, S. Guignard, R. Awadallah, and D. R. Thompson, "Local and non-local curvature approximation: a new asymptotic theory for wave scattering," *Waves in Random Media*, vol. 13, no. 4, pp. 321–338, 2003.

[10] T. M. Elfouhaily and J. T. Johnson, "Extension of the local curvature approximation to third order and full tilt invariance," accepted by *Waves in Random and Complex Media*, 2006.

[11] C. A. Guérin, G. Soriano, and T. Elfouhaily, "Weighted curvature approximation: numerical tests for 2D dielectric surfaces," *Waves in Random Media*, vol. 14, pp. 349–363, 2004.

[12] Johnson, J. T., and M. Zhang, "Theoretical study of the small slope approximation for ocean polarimetric thermal emission," *IEEE Trans. Geosc. Remote Sens.*, vol. 37, pp. 2305–2316, 1999.

[13] Johnson, J. T. and Y. Cai, "A theoretical study of sea surface up/down wind brightness temperature differences," *IEEE Trans. Geosc. Remote Sens.*, vol. 40, pp. 66–78, 2002.

[14] *Maui High Performance Computing Center World Wide Web Site*, on the World Wide Web at *http:www.mhpcc.edu*.

[15] Durden, S. L. and J. F. Vesecky, "A physical radar cross-section model for a wind driven sea with swell," *IEEE J. Oceanic Eng.*, vol. OE-10, pp. 445–451, 1985.

[16] Johnson, J. T., R. T. Shin, J. A. Kong, L. Tsang, and K. Pak, "A numerical study of the composite surface model for ocean scattering," *IEEE Trans. Geosc. Remote Sens.*, vol. 36, no. 1, pp. 72-83, 1998.

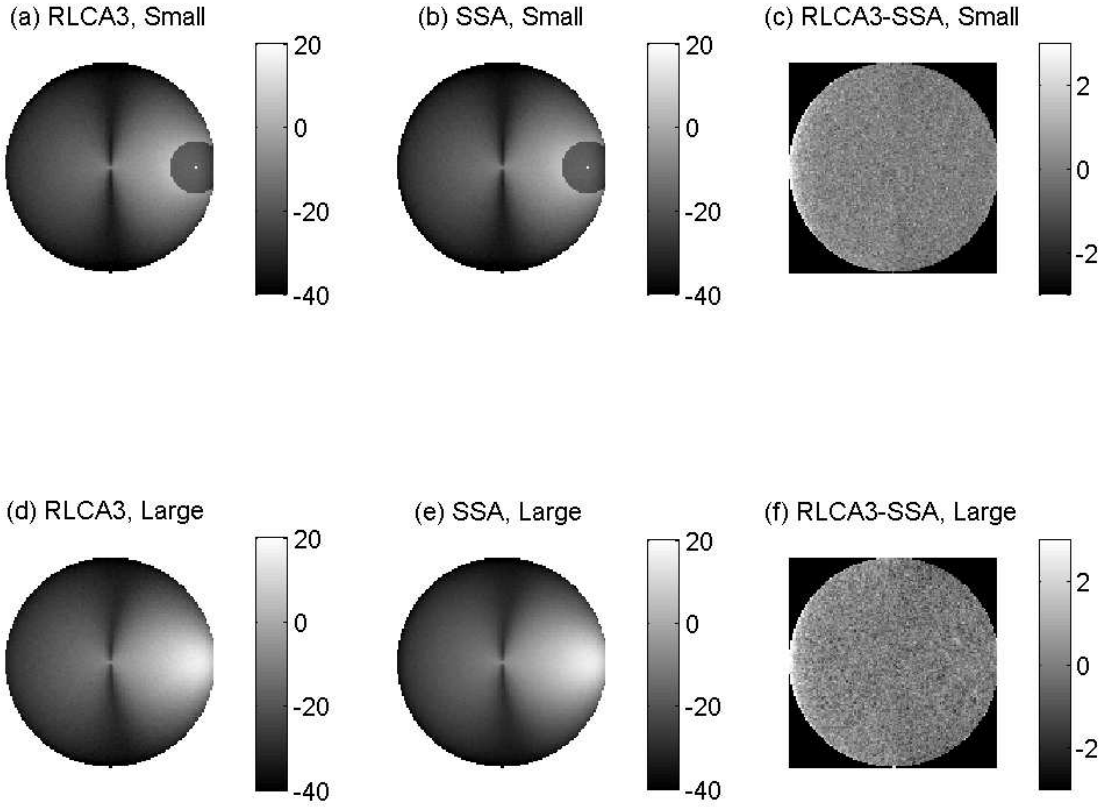

Fig. 1. Comparison of RLCA3 and SSA bistatic scattering patterns: HH polarization

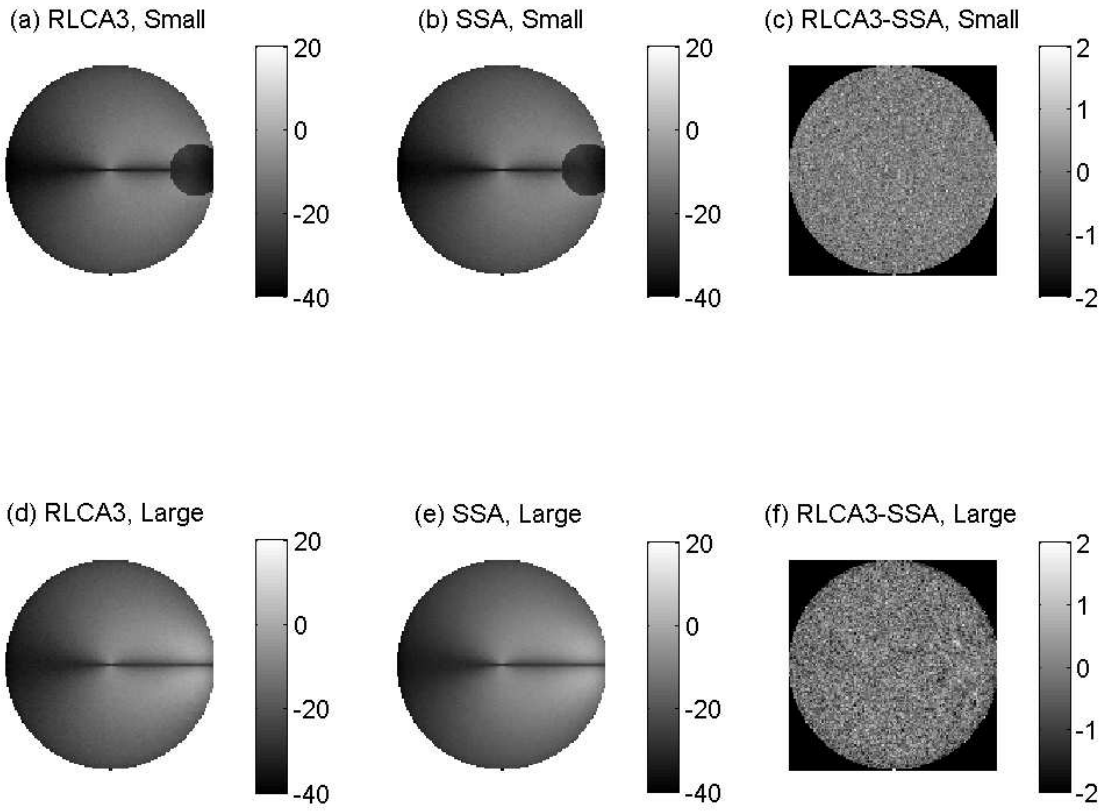

Fig. 2. Comparison of RLCA3 and SSA bistatic scattering patterns: VH polarization

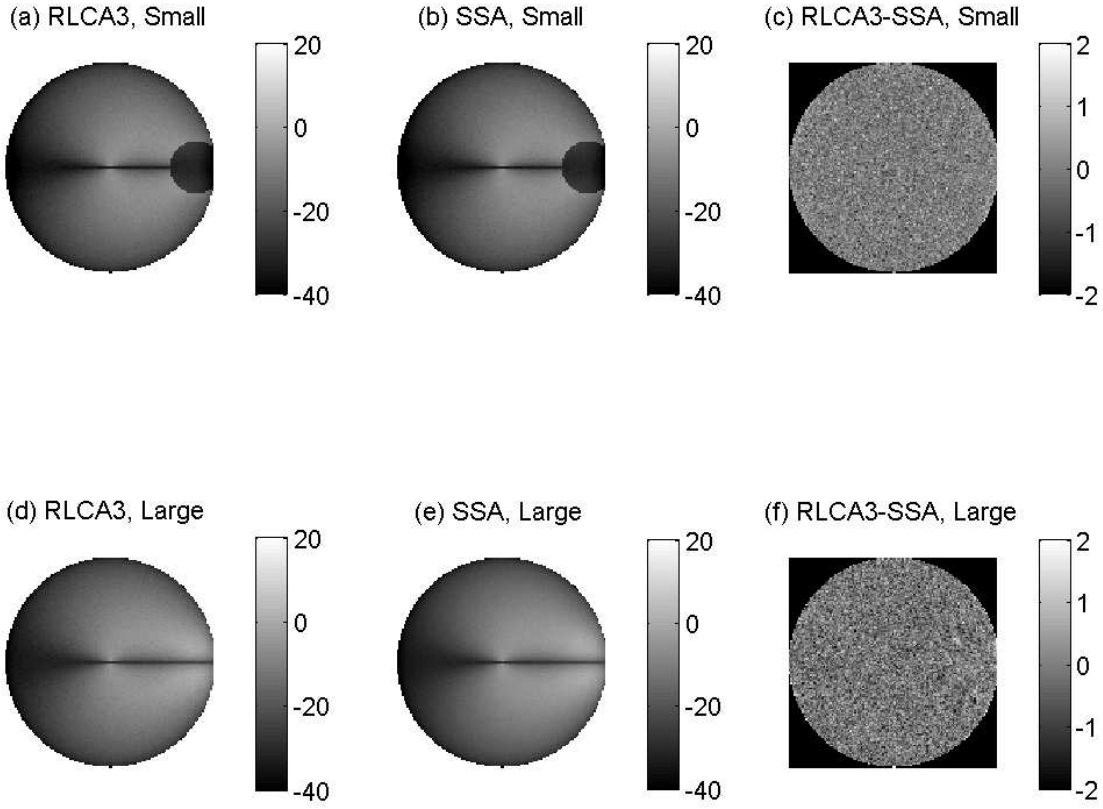

Fig. 3. Comparison of RLCA3 and SSA bistatic scattering patterns: HV polarization

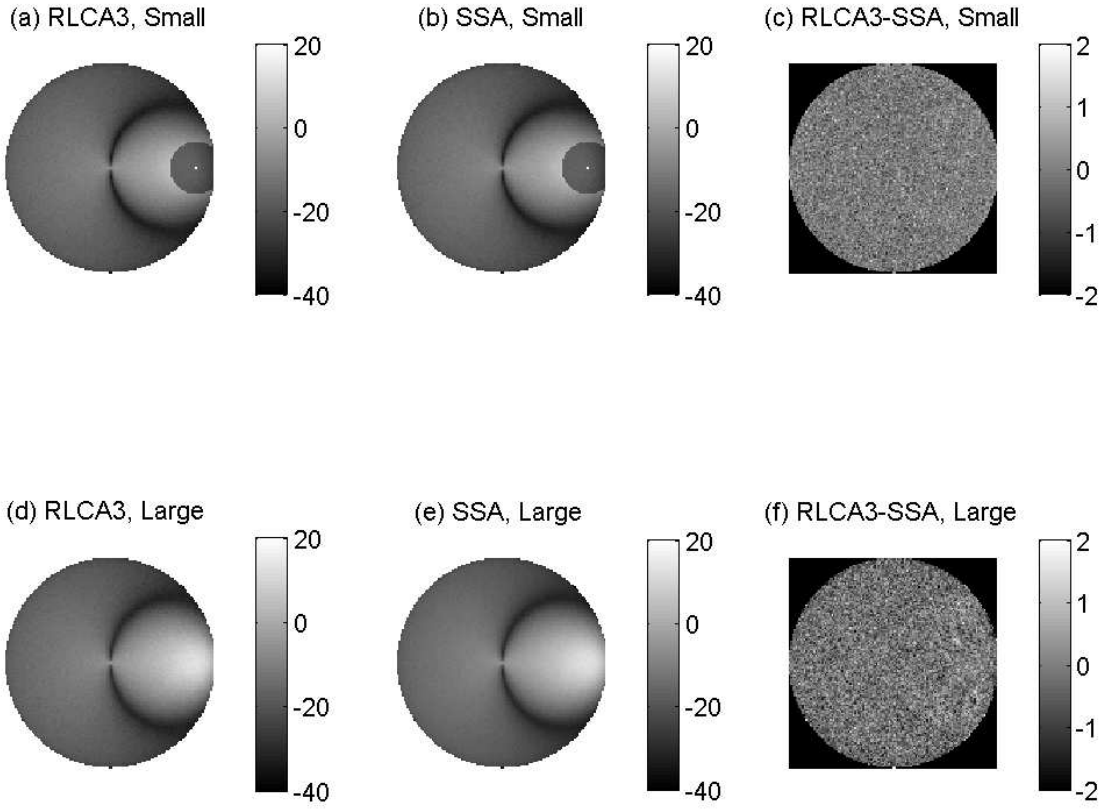

Fig. 4. Comparison of RLCA3 and SSA bistatic scattering patterns: VV polarization

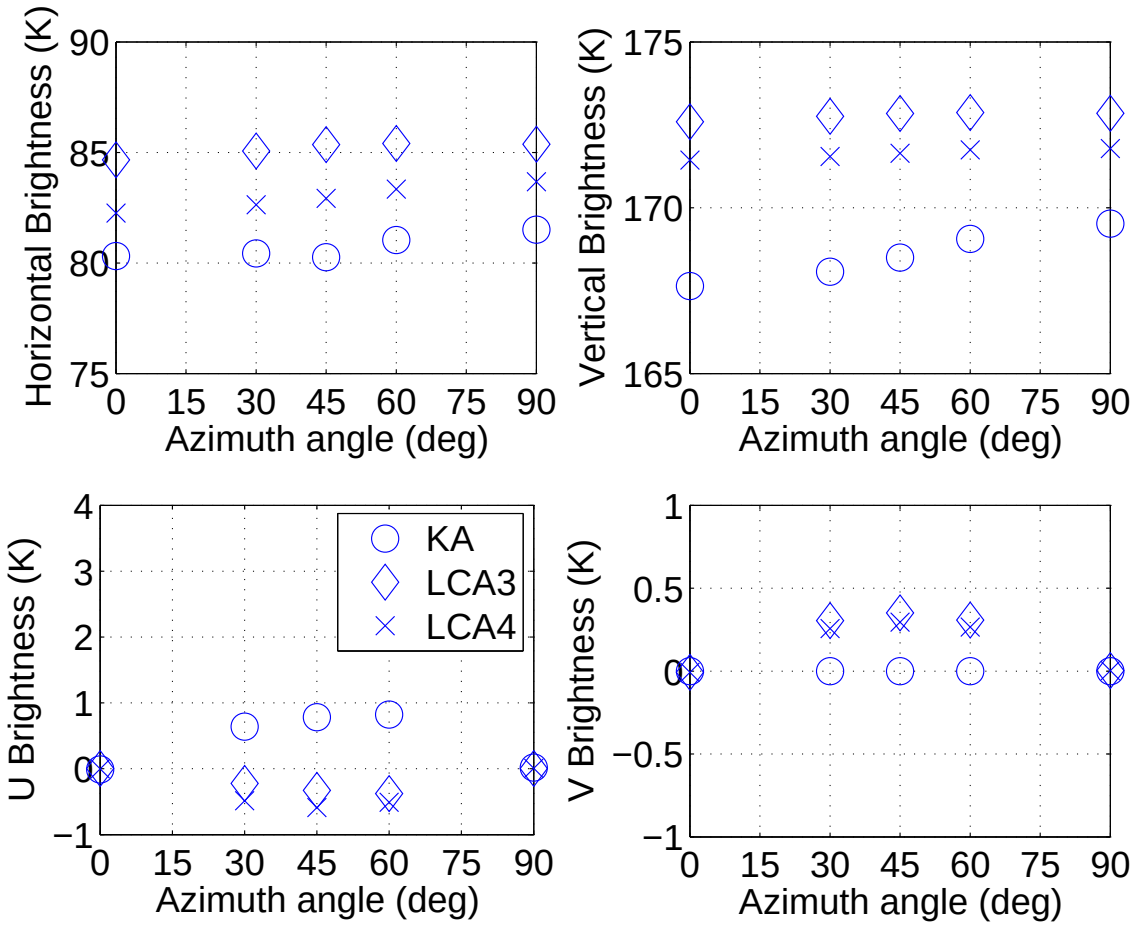

Fig. 5. Comparison of KA, LCA3, and LCA4 predictions for large height surface emission

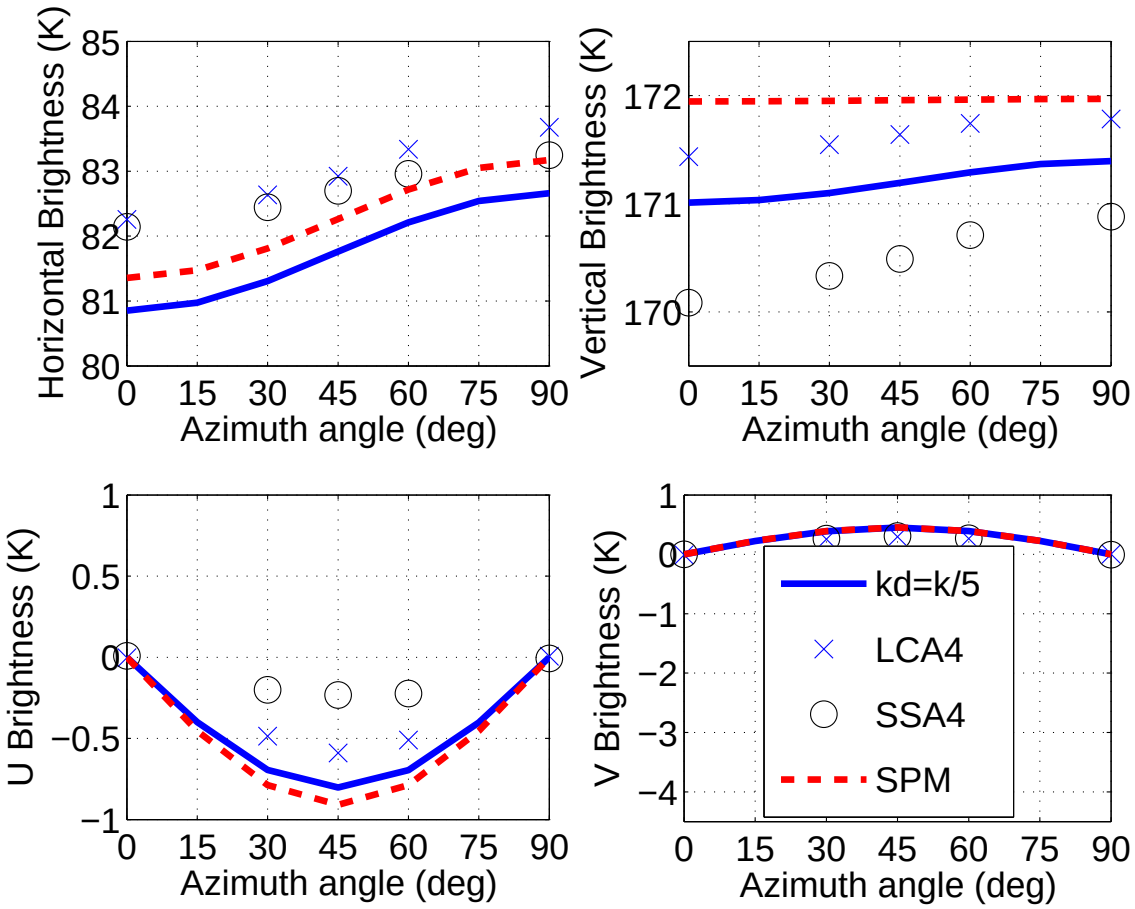

Fig. 6. Comparison of RLCA3, SSA, two-scale, and SPM model predictions, large height case. Two-scale model predictions were computed using a cutoff wavenumber of $k_0/5$, where k_0 is the electromagnetic wavenumber.

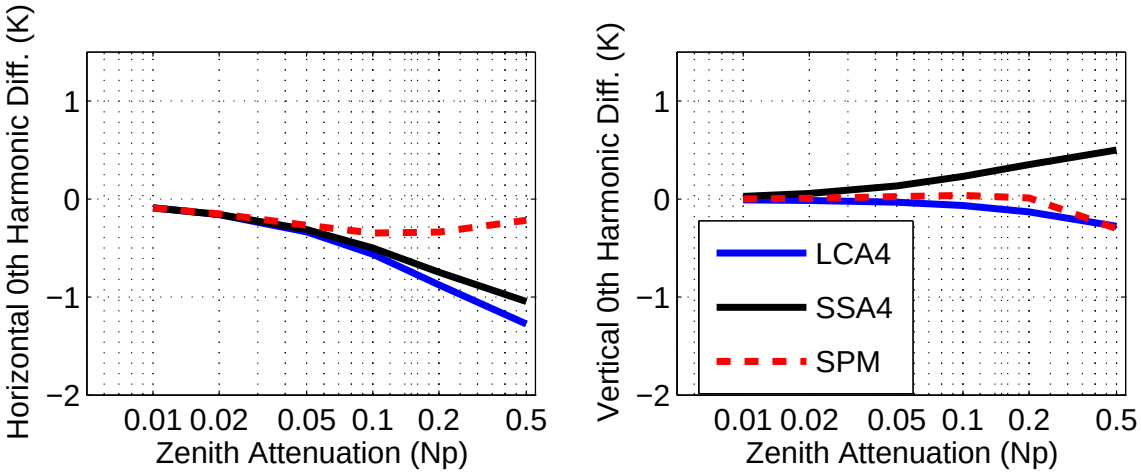

Fig. 7. Zeroth azimuthal harmonic differences of reflected downwelling brightness, large height case; two-scale model ($k_d = k_0/5$) predictions are subtracted from the models indicated

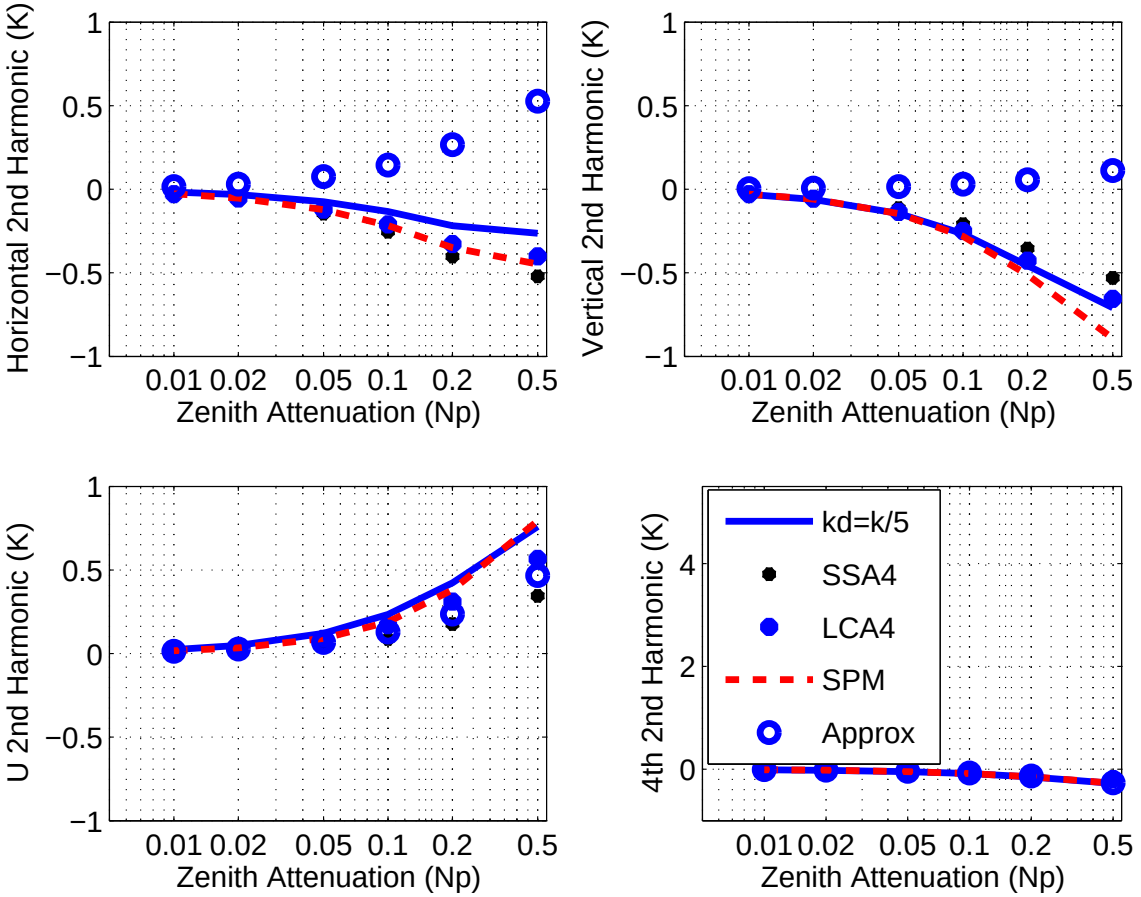

Fig. 8. Second azimuthal harmonics of reflected downwelling brightnesses from the RLCA3, SSA, two-scale, SPM, and simple approximation models, large height case